Direct Ammonia Solid Oxide Fuel Cell Stack: Modelling and Experimental Validation

Emanuele Martinelli¹ Michele Bolognese¹ Nirmala Nirmala² Narges Ataollahi³ Matteo Testi¹

¹Fondazione Bruno Kessler, Research Center, Italy, {emmartinelli, mbolognese, testi}@fbk.eu

²Modelon Deutschland GmbH, Hamburg, Germany, nirmala.nirmala@modelon.com

³Department of Civil, Environmental and Mechanical Engineering, University of Trento, Italy,

narges.ataollahi@unitn.it

Abstract

Interest in ammonia as an energy carrier is growing due to its superior storage and transport properties compared to hydrogen. The objective of this work is to construct a useful tool for predicting the behavior of a solid oxide fuel cell (SOFC) stack fed directly with ammonia. This configuration is particularly interesting because the internal cracking of ammonia eliminates the need for an external cracker, thus reducing the overall cost of the system. The ammonia decomposition reaction was implemented in the anode channel of the stack and calibrated against literature results. The model was then validated in the ohmic region only by calculating the area specific resistance (ASR) and comparing the results with experimental data collected at the Bruno Kessler Foundation (FBK) laboratory. This SOFC model can therefore be used as a starting point for the analysis of a scale-up application.

Keywords: Solid oxide fuel cell, High temperature fuel cell, Internal ammonia cracking, Experimental validation

1 Introduction

With the European Union setting a target of zero greenhouse gas emissions by 2050 (EuropeanCommission 2022), the need for sustainable, low-impact solutions for energy generation has become critical. According to the 1.5 °C scenario outlined by the International Renewable Energy Agency (IRENA 2024), hydrogen will account for up to 14% of total final energy consumption. It will also play a central role in the decarbonisation of hard-todecarbonise industries (e.g., steel, chemicals and refineries), in the storage of excess renewable energy to provide flexibility to the grid, and in supporting long-distance transport directly or via hydrogen carriers. Among the potential hydrogen carriers, ammonia is a promising option due to its carbon-free nature and high hydrogen storage capacity; it offers favourable gravimetric (17.88 %wt) and volumetric (10.7 kg_{H₂} per 100 l) hydrogen densities, and, in its liquid form, it achieves a volumetric energy density of 12.9 MJ/l, surpassing that of liquid hydrogen at 8.6 MJ/l. The ammonia liquefaction process requires less extreme conditions, achieved at -33.3 °C at atmospheric pressure or about 10 atm at ambient temperature (Wang et al. 2022), making ammonia a better solution for long distance energy transport. It is also the second most produced and traded chemical in the world, 70% of which is used as a base for fertilisers and the remainder as an input for industrial processes, such as a refrigerant or in the manufacture of synthetic fibres, plastics and explosives (IEA 2021).

Fuel cells are electrochemical devices that convert chemical energy directly into electrical energy, without the need for combustion or intermediate conversion into mechanical energy; this makes them more efficient than traditional combustion generators. The basic working principle of fuel cells is the electrochemical reaction between a fuel and an oxidant, typically hydrogen and oxygen, respectively. In a solid oxide fuel cell (SOFC), the oxygen supplied to the cathode is reduced to form oxygen ions (O²⁻), which then flow through the electrolyte to the anode. There, the O²⁻ ions combines with hydrogen to form water, releasing two electrons that will flow to the cathode through an external electrical circuit (reaction 1). The hydrogen required at the anode can be supplied directly or can be produced by the cracking of more complex fuels, such as methane and ammonia. The primary advantage of SOFCs is that they operate at high temperatures; this creates an environment in which complex fuels (with ammonia being the fuel of choice in this particular case study) spontaneously decompose at the anode electrolyte, releasing hydrogen directly into the anode channel (see the configuration on the right-hand side of Figure 1). If an external fuel processor were needed to extract hydrogen from the fuel, the system's complexity would increase, and the costs would rise concomitantly.

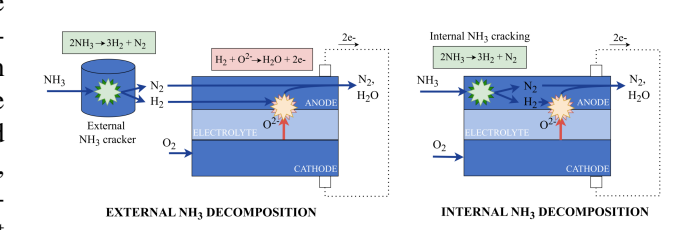


Figure 1. Ammonia decomposition in different configuration (indirect on the left, direct on the right) of a solid oxide fuel cell system.

In the present case study, a model of a short SOFC stack operating at elevated temperatures and fed directly with ammonia was developed and validated; this configuration is of particular interest because it allows the direct decomposition of ammonia in the anode channel, according to the endothermic reaction 2 ($\Delta H = 46.18 \ kJ/mol$), without the need for an external cracker as required in indirect ammonia fuel cells (Lyu et al. 2023).

$$H_2 + O^{2-} \to H_2O + 2e^-$$
 (1)

$$NH_3 \to \frac{3}{2}H_2 + \frac{1}{2}N_2$$
 (2)

Different equations were proposed to quantify the ammonia conversion performance over different catalysts (Wan et al. 2021; Zheng et al. 2023); Kishimoto et al. have developed and validated Equation 3, on which is presented the ammonia decomposition model in subsection 2.1 (Kishimoto et al. 2017). This reaction model was then implemented in the anode channel of the substack to obtain the final direct ammonia stack model. The stack model was then validated with experimental data collected on a test bench provided by SolydEra S.p.A. at the Fondazione Bruno Kessler laboratory; the stack consists of 6 cells connected in series with an active surface of 80 cm². The values of the operating parameters have been obtained from the experimental setup, while, for reasons of confidentiality, the material structure and the geometric organisation of the stack used in the model have been taken from literature works. To determine the applicability of the model and verify its robustness, the discrepancy between the experimental and simulation results was calculated for each test described in subsection 2.4.

This work focuses on understanding ammonia-based energy conversion and also provides a practical tool for analysing the operation of a SOFC stack that does not require the use of an expensive external cracker. This tool can also be used for future scale-up applications within a complex Balance of Plant (BoP).

2 Methods

The methodology adopted in this work is investigated using the Modelica language and Modelon Impact as tool. Modelica is an open-source language for modelling complex systems covering multi-domains such as mechanical, electrical, thermal and control. Modelon Impact is a cloud-native Modelica modelling and simulation platform, which offers a suite of libraries with preconfigured and validated components to help users get started in building their systems. In this work, building blocks from Modelon's Fuel Cell Library (FCL) have been employed. The FCL is primarily used for modelling, simulation, analysis, and control of fuel cell design and operation.

To build a direct ammonia solid oxide fuel cell (SOFC) stack model, it is first necessary to create a suitable ammonia medium and calibrate the ammonia decomposition reaction model. This reaction model is then implemented

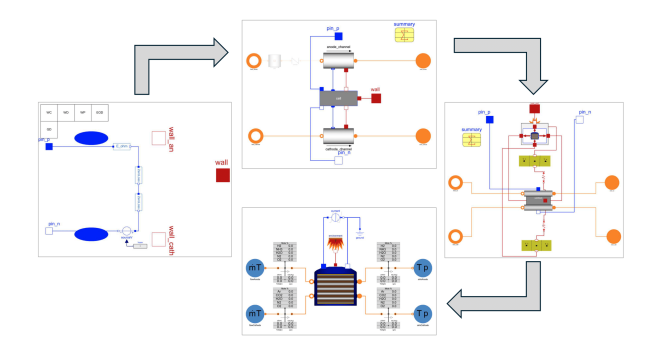


Figure 2. Cell, substack, stack and stack simulation models. Arrows indicate the dependence of nested models, from innermost to outermost models.

in the anode channel of the substack model, which also comprises the cell and cathode channel models. The cell model calculates the cell voltage by estimating the area specific resistance ASR [Ω/cm^2]; the values of the parameters used in Equation 10 are found experimentally. The substack model is encapsulated within the stack model, where the heat loss characteristics are defined. Finally, a stack simulation model is created to define the boundary conditions from the experimental setup and to validate the stack model. The nested structure used for the stack validation is shown in Figure 2.

2.1 Ammonia Decomposition Reaction

A medium containing ammonia (H_2 , NH_3 , H_2O , N_2 and O_2) was created with thermodynamic properties taken from the Modelon NASA database (McBride, Zehe, and Gordon 2002) and compared to the NIST database (NIST 2023) for verification. An ammonia decomposition model was then subsequently created and validated with the reaction channel model shown in Figure 3.

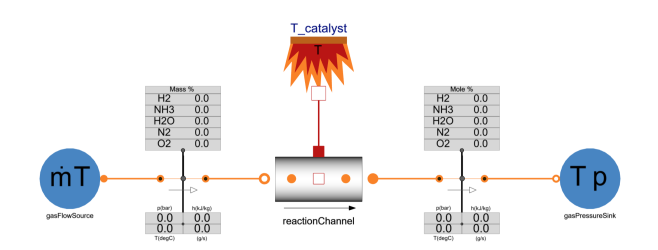


Figure 3. Discretised reaction channel model created to calibrate the ammonia decomposition reaction.

The ammonia decomposition reaction model, embedded within the reaction channel, was built on the basis of the work of Kishimoto et al., who validated Equation 3 against experimental results varying the catalyst temperature, ammonia mass flow rate or hydrogen mole fraction in the input fuel (Kishimoto et al. 2017).

$$R_{dec} = CE \ S_{Ni-pore} \ A^{Ni-pore} \ \exp\left(-\frac{E}{RT}\right) \cdot \left(p_{NH_3}\right)^a \left(p_{H_2} + c\right)^b \tag{3}$$

For the reaction calibration, the unit volume reaction rate R_{dec} $[mol/m^3s]$ was calibrated with the conversion efficiency parameter CE [-]. The other coefficients were chosen according to the calibration performed by (Kishimoto et al. 2017), assuming the same material properties as the Ni-YSZ catalyst used in the validation process; this material is one of the most commonly used in commercially available SOFC stacks, which makes it relevant to the case study. To obtain the decomposition reaction rate in [mol/s], R_{dec} is multiplied by the catalyst volume V_{cat} $[m^3]$, calculated as $V_{cat} = V_{ch} \cdot f_{cat}$, where f_{cat} [-] is the ratio of catalyst volume to channel volume. As the ammonia decomposition reaction is endothermic, (Kishimoto et al. 2017) also provides an estimate of the heat flow Q_{reac} [W] withdrawn from the reaction with Equation 4.

$$Q_{reac} = \Delta H R_{dec} V_{cat} \tag{4}$$

The change in enthalpy $\Delta H \ [J/mol]$ caused by the decomposition reaction is evaluated as $\Delta H = -40265.95 - 24.23214T + 0.00946T^2$, where $T \ [K]$ is the fluid temperature within the channel for each discretization.

The geometric and operational parameters considered for the reaction channel model are given in Table 1. The assumptions that were considered during the modelling design phase are reported in the following list:

Table 1. Geometrical and operating parameters adopted in the reaction calibration model.

Var.	Value	Unit	Description
$N \\ m_{flow} \\ p \\ T_{cat} \\ D \\ L \\ f_{cat} \\ \varepsilon$	10 1.266e-6 101325 600, 650, 700 8.3 10, 20, 40 0.01 2.5e-5	kg/s Pa °C mm mm	discretization number NH ₃ mass flow system pressure catalyst temperature channel diameter catalyst length catalyst fraction pipe roughness

- the reaction takes place only within the catalyst volume V_{cat} , which is considered fully active, and at a constant temperature T_{cat} [°C] along the channel.
- the ammonia mass flow m_{flow} [kg/s] is calculated from the volume flow V_{flow} [ml/min] under normal conditions using the ideal gas law;
- D [m] is the equivalent diameter, calculated from the cross-section of the rectangular channel;
- the pressure drop dp [Pa] along the channel is calculated for all flow regimes with Equation 5, where the friction factor λ is found from the Reynolds number Re and the absolute surface roughness ε ;
- the heat transfer coefficient α [W/m^2K] is calculated over the entire Reynolds number (Re) range and for

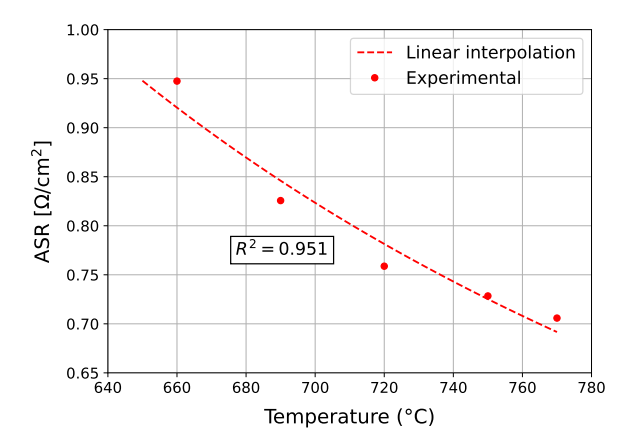


Figure 4. Experimentally found ASR values and values obtained from Equation 10 are plotted against average stacked temperature.

each discretisation with the Equation 6, where Nu_{ave} represents the average Nusselt number for the section and λ [W/mK] is the conductivity of the fluid;

$$dp = \lambda(Re, \varepsilon) \frac{L}{D} \rho \frac{v^2}{2} sign(v)$$
 (5)

$$\alpha = \frac{Nu_{ave} \,\lambda}{D_{hvd}} \tag{6}$$

2.2 Cell Model

The FuelCell.Membranes.SOFC.Simplified cell model includes mass flow, electrical and thermal connectors. The former are used to import data on the pressure, temperature and composition of the media flowing into the anode and cathode channels from the substack model at a higher level; these data relate only to the amount of gases required for the hydrogen oxidation reaction to occur (i.e., Reaction 1) and are then used to calculate the thermodynamic state of these gases at the electrode-electrolyte interface. The electrical connectors are used to construct the electrical circuit of the cell.

The electrical circuit is built within the cell to allow the calculation of the cell voltage V_{cell} [V] with the Equation 7; the circuit is represented by two pins, a block that calculates the Nernst voltage E_0 with Equation 8 and a block that calculates the voltage drop due to internal losses in the cell ΔV_{losses} .

$$V_{cell} = E_0 - \Delta V_{losses} = E_0 - (V_{act} + V_{ohm} + V_{conc})$$
 (7)

$$E_0 = -\frac{1}{n_e F} \left(g_{reaction} + RT_{cell} \ln \left(\frac{p_{H_2O}}{p_{H_2} \cdot p_{O_2}^{0.5}} \right) \right)$$
(8)

According to Andersson et al., the internal cell losses can be estimated by Equation 9, where $ASR(T) \left[\Omega/cm^2\right]$ is the area specific resistance of the cell, which depends only

on the temperature of the cell (Andersson et al. 2011). E_a [J/mol] is an activation energy representing all the possible losses the current experiences as it passes through the stack's electrical circuit, while ASR₀ is the reference area specific resistance measured at the reference temperature T_0 [K]. This simplification is necessary in this case study because the materials used in the SOFC stack are covered by trade secrets, so using the parameters and coefficients required by the specific activation, ohmic and concentration loss models would have been misleading.

$$V_{cell} = E_0 - ASR(T) \cdot j_{cell} \tag{9}$$

$$ASR(T) = ASR_0 \cdot \exp\left[\frac{E_a}{R} \left(\frac{1}{T_{cell}} - \frac{1}{T_0}\right)\right]$$
 (10)

$$ASR(T) = ASR_0 \cdot \exp\left[\frac{E_a}{R} \left(\frac{1}{T_{cell}} - \frac{1}{T_0}\right)\right]$$
(10)
$$\ln ASR = \frac{E_a}{R} \frac{1}{T} + \left(\ln ASR_0 - \frac{E_a}{RT_0}\right) \rightarrow y = mx + q$$
(11)

The experimental ASR_0 , E_a and T_0 values, reported in Table 2, are obtained by solving Equation 11 for the experimental points given in Figure 4 (Zendrini et al. 2021), where the average furnace temperature is determined by averaging the anode and cathode gas temperatures at the inlet and outlet. This average value is considered to be representative of the thermal conditions of the stack for ASR calculations, but it is dependent on the internal geometry and materials of the stack. Therefore, it cannot be validated with relevant results in the current case study.

Table 2. Values of the coefficients used in the ASR(T) equation for the calculation of cell internal losses when the stack model is run with pure ammonia.

	Unit	Experimental	Simulation
ASR_0	Ω/cm^2	0.92	0.4
E_a	kJ/mol	21.028	21.028
T_0	$^{\circ}C$	660	660

The simulation values in Table 2 are found following the procedure described in subsection 3.2. It should be noted that the activation energy is kept constant, but ASR_0 varies; this allows large deviations in the cell voltage trend to match experimental curves, as shown in Figure 8.

2.3 **Substack Model**

The FuelCell.Stacks.SOFC.SubStack model includes the anode, elementary cell and cathode channels. These models are then connected thermally, electrically and in terms of mass flow; gas streams are introduced into the anode, where ammonia is decomposed, and cathode channels. The mass ports connect the two channels to the cell, only transporting the necessary species for the membrane reaction. The excess gas then flows through the channel and out of the stack. The thermal ports establish the electrodes' temperature, with a third port assigned to the cell temperature and excess heat; this heat flow must

Table 3. Geometrical parameters adopted for the description of the substack model (Omer et al. 2023).

Var.	Value	Unit	Description	
N	10	-	number of discretizations	
n_{cells}	6	-	number of cells	
A_{cell}	80	cm^2	active cell area	
w_{cell}	7.3	cm	cell width	
l_{cell}	10.96	cm	cell length	
$h_{an,ch}$	0.4	mm	anode channel height	
$h_{an,el}$	0.66	mm	anode electrode thickness	
h_{el}	0.02	mm	electrolyte thickness	
$h_{cath,el}$	0.03	mm	cathode electrode thickness	
$h_{cath,ch}$	0.8	mm	cathode channel height	
Cylindrical analogy				
$d_{an,ch}$	6.1	mm	anode channel diameter	
$d_{cath,ch}$	8.6	mm	cathode channel diameter	

be dissipated through the end plates and side wall of the stack and transmitted to the stack-level heat box model.

The performance of the stack is significantly influenced by the geometrical dimensions of the channels. Due to the confidential geometrical structure, the stack configuration studied by Omer et al. is considered as a reference (Omer et al. 2023): the materials constituting the anode, electrolyte and cathode electrodes are among those most commonly used in commercial applications (Ni-YSZ, YSZ and LSM, respectively), and the geometrical characteristics are close to the external appearance of the stack present in the FBK laboratory. The geometrical parameters adopted in this case study are reported in Table 3.

It should be noted that the active cell area presented in the reference case is 100 cm², so the cell size has been scaled to match the 80 cm² of the case study, while maintaining the structure along the cell axis perpendicular to the flow direction. The fraction of catalyst in the anode channel f_{cat} , presented in subsection 2.3 for the ammonia decomposition reaction, is unknown for the test bench, but

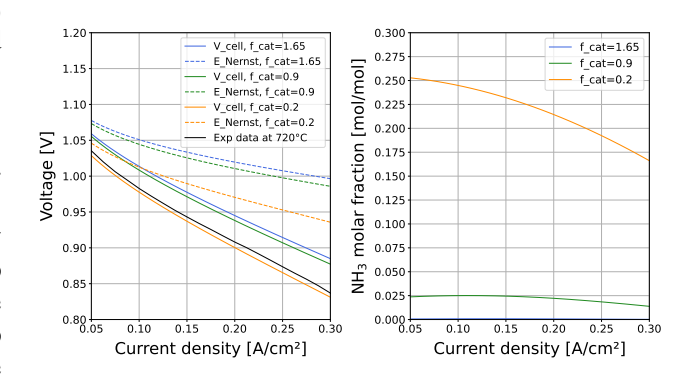


Figure 5. Simulated Nernst voltage and cell voltage (left) of the stack model at 710 °C as a function of varying catalyst fractions within the anode channel. Corresponding ammonia molar fraction at the anode outlet (right).

it has a strong influence on the H_2 availability, which then determines the Nernst voltage (Equation 8). The volume of the anode electrode V_{cat} was calculated using the data provided in Table 3 following the procedure described in subsection 2.1 on ammonia decomposition and neglecting the catalyst porosity. The result, $f_{cat} = 1.65$, leads to the almost complete ammonia conversion, causing issues when calculating the Nernst voltage, as shown in Figure 5: the higher the ammonia converted, the more hydrogen available to the cell, resulting in an upward shift of the polarisation curve. Therefore, $f_{cat} = 0.2$ is used; calibrating this parameter would have been possible also by measuring the ammonia outlet of the anode channel with a mass spectrometer.

The substack model uses Equation 5 for the pressure drop calculation, so the calculation of the Reynolds number *Re* is greatly influenced by the anode and cathode channel diameters in Table 3; they are determined by cylindrical analogy, based on the channel's height only, ignoring the electrode's height, which is the same procedure used for the ammonia decomposition reaction calibration in subsection 2.1.

2.4 Stack Model

The experimental test bench consists of six planar oxygenion conducting cells electrically connected in series. In its nominal state, the stack operates at ambient pressure, 0.78 V cell voltage, and 400 A/cm² current density for a total nominal power of 150 W. The stack is enclosed in a furnace containing electric heaters to bring the temperature of the air near the stack to a set temperature T_{set} , which is then maintained by a proper temperature control; the anodic and cathodic gases are heated to this temperature before entering the stack. Therefore, no thermal insulation has been considered in the stack model and both gases have the set temperature presented in Table 4.It would be possible to calculate dispersion through the furnace insulation at a later stage by taking into account the difference between the average furnace temperature and the ambient temperature. However, this is beyond the scope of this study.

The FuelCell.Stacks.SOFC.Stack model had to be simplified because it only accepts a minimum number of substacks equal to 2, whereas in the case study there is only a short stack of 6 cells. Therefore, the $nbr_{substack}$ dependent variables are simplified, and the manifold models are removed. This stack model then extends the electrical, thermal and mass flow connections and incorporates the substack model and the heat box model, which would represent the conductive, convective and radiative heat losses from the furnace to the environment.

The operating conditions adopted during the experimental analysis are reported in Table 4; the performance of the stack is evaluated for the five temperatures set within the ohmic region of the polarisation curve, i.e., where the voltage decreases with a linear trend, thus from J=0.05 A/cm^2 to J=0.30 A/cm^2 in Figure 6.

Table 4. Operating conditions adopted for the tests conducted on the test bench in the FBK's laboratory.

Var.	Value	Unit	Description
$T_{set,1}$	650	$^{\circ}C$	furnace set temperature
$T_{set,2}$	680	$^{\circ}C$	furnace set temperature
$T_{set,3}$	710	$^{\circ}C$	furnace set temperature
$T_{set,4}$	740	$^{\circ}C$	furnace set temperature
$T_{set,5}$	760	$^{\circ}C$	furnace set temperature
$\overline{U_{fuel}}$	0.75	-	utilization rate at 32A
U_{air}	0.10	-	utilization rate at 32A
\dot{V}_{NH_3}	1.189	Nl/min	volume flow rate
\dot{V}_{air}	31.876	Nl/min	volume flow rate
\dot{m}_{NH_3}	1.506e-5	kg/s	mass flow rate
\dot{m}_{NH_3}	6.862e-4	kg/s	mass flow rate

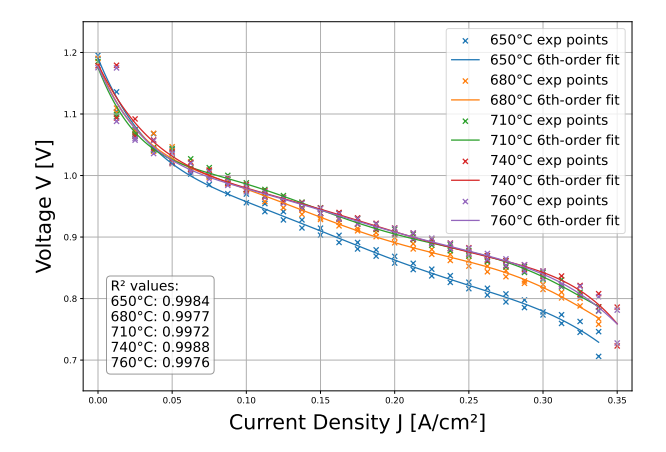


Figure 6. These are the experimental polarisation curves obtained from operating the test bench. The continuous lines were obtained by interpolating the average values of the experimental points using a sixth-order polynomial equation. The coefficient of determination R^2 for each temperature is shown to demonstrate how well the fitted values represent the experimental data.

3 Results and Discussion

The aim of the dynamic simulations, conducted for each of the models presented in the previous subsections, is to obtain the same performance as that obtained experimentally, with the smallest possible relative error $(\mathcal{E}_{\%})$ for each time step.

$$\varepsilon_{\%} = \left| \frac{V_{exp} - V_{sim}}{V_{exp}} \right| \tag{12}$$

3.1 Ammonia Decomposition Reaction Calibration

The amount of converted ammonia was calculated by transforming the NH₃ volumetric flow into mass flow using the ideal gas law under normal conditions. This step was necessary to compare the simulation results with those found in the literature; the conversion percentages are derived as the ratio between the decomposed ammo-

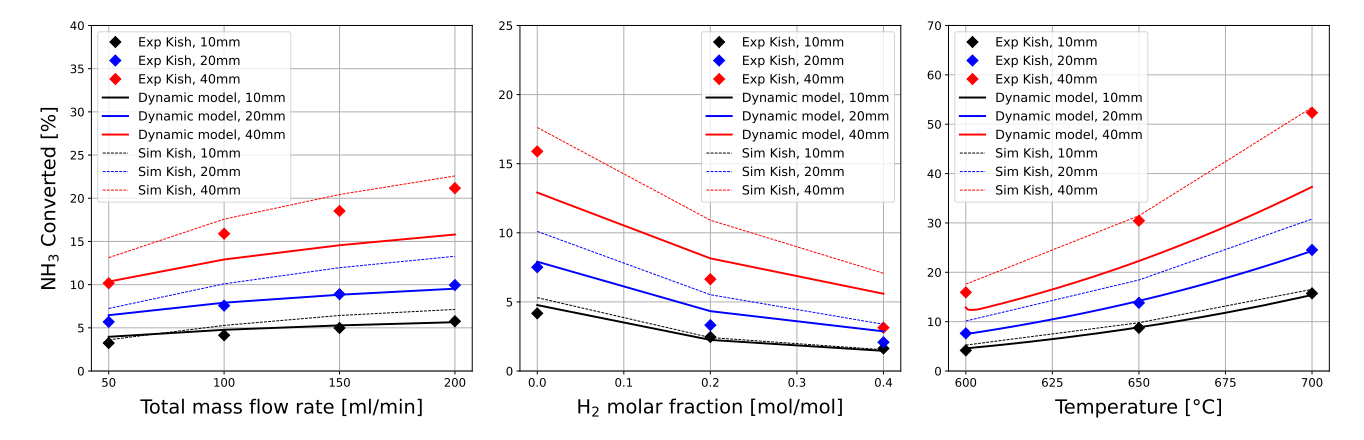


Figure 7. Comparison between the performance of the ammonia decomposition model and that obtained from simulations of the same operating conditions as described in the literature (Kishimoto et al. 2017). Discrepancies are calculated considering the experimental results with Equation 12, for both the simulation results obtained by Kishimoto et al. and the results obtained with the dynamic reaction channel model in the current case study.

nia volumetric flow and the incoming one. The calibration process results, shown in Figure 7, are obtained using CE = 0.85 (Equation 3). It is important to note that the discrepancy was obtained by comparison with the experimental results found in the reference article and not those from their simulations (Kishimoto et al. 2017).

It is evident that the reaction model aligns with the ammonia conversion curve for catalyst lengths of 10 mm and 20 mm, exhibiting smaller discrepancies compared to the results reported in (Kishimoto et al. 2017). However, higher discrepancies are observed when the catalyst is 40 mm long. This discrepancy, indicating a reduced conversion performance with a catalyst length of 40 mm, can be attributed to the observation that the gas exhibits increased dilution within the terminal segment of the catalyst and that the increased presence of hydrogen also reduces the ammonia conversion rate R_{dec} . This phenomenon could be attributed to the application of a lumped pseudo-1D model; however, this assertion needs to be validated by reproducing the experimental apparatus and also verifying that no potential factor has been overlooked by the authors of this case study.

This calibration process is considered a necessary step in obtaining a reaction that, when incorporated into the final SOFC stack model, can simulate the internal ammonia cracking.

3.2 Choice of ASR Values

It is important to comment on the value of the ASR(T) coefficients that are used in the stack model. The experimental values are derived from the polarisation curve in the linear region, thus making $ASR_{exp}(T)$ dependent only on the average temperature of the stack, as shown in Figure 4. Consequently, all types of losses that result in a cell voltage drop from the open-circuit voltage value $OCV = E_0|_{I=0A}$ are included. However, it has been observed that, during the simulation, the cell model iteratively solves Equation 8 using the local values of partial

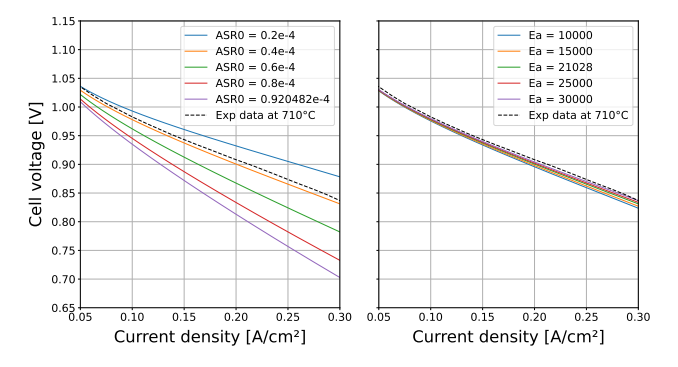


Figure 8. The two plots show a sensitivity analysis performed for operating the stack at 710 °C while keeping E_a , in the left plot, and ASR_0 , in the right plot, at the experimental values.

pressures, which are determined by the cell performances: higher current requires higher hydrogen oxidation, thus the Nernst voltage decreases (see Figure 5). This decreasing effect is already taken into account in the calculation of the derivative of the polarisation curve to be calculated, so if the experimental values (Table 2) of ASR_0 and E_a were used in the model, the internal losses of the cell would be overestimated. A sensitivity analysis is presented in Figure 8 to explain the phenomenon above.

3.3 Stack Validation

Once the most influential parameters presented in subsection 2.4 are set, the stack operation is simulated under the operating conditions shown in Table 4. In Figure 9, V_{cell} values obtained from the dynamic simulation of the stack model are compared to the V_{cell} values derived from the polynomial fitting of experimental data in the ohmic current density range; the graph is represented with continuous curves to demonstrate, moment by moment, the discrepancy between the model's predictions and the actual cell voltage values. The stack model is considered validated, as the maximum value of the discrepancy is 2.18% at $T=760\,^{\circ}\text{C}$.

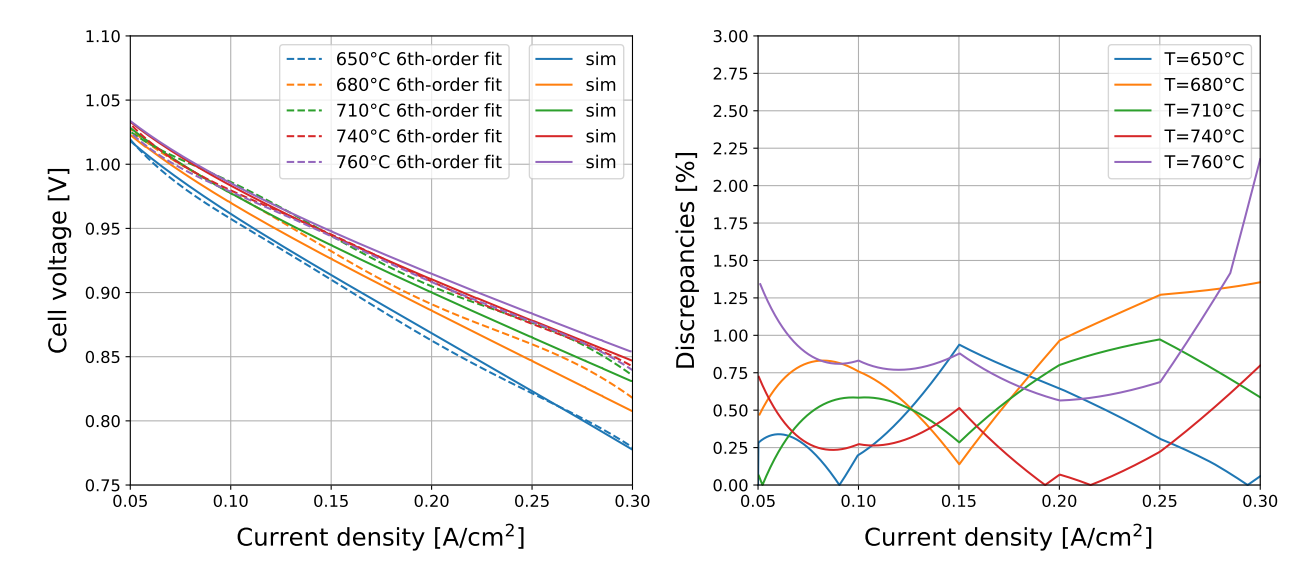


Figure 9. Comparison between the interpolated experimental polarisation curves and those obtained from the dynamic simulation of the stack model over the selected ohmic range of current density. The discrepancy values (right) diagram are obtained with Equation 12 for each point on the polarisation curve, with a maximum value of 2.18% at T=760 °C.

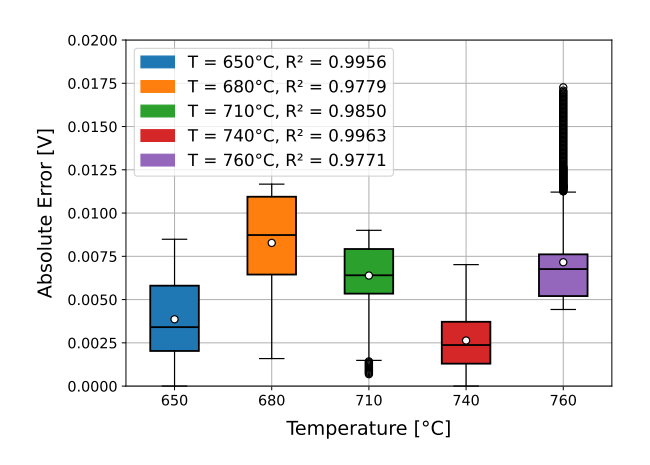


Figure 10. Boxplot of absolute voltage error distribution across temperatures. Each box shows the median, interquartile range and variability of the error between experimental and simulated values, with the mean error represented by a white circle.

Figure 10 shows an analysis of the absolute error distribution to evaluate the performance of the model at different operating temperatures; the coefficient of determination R^2 has also been calculated and plotted for each temperature to help quantify the fit of the model to the experimental data. High R^2 values, such as 0.9956 at 650 °C and 0.9963 at 740 °C, indicate that the model can capture the variability in the experimental data. Lower values, such as 0.9779 at 680 °C and 0.9771 at 760 °C, are still considered good, as the model was built with some general assumptions that can be further investigated to improve the overall performance.

Figure 11 shows an overview of the cell performance in different sections along the longitudinal axis in terms of cell temperature and amount of ammonia left at the end of the anode channel. In fact, as explained in subsection 2.1,

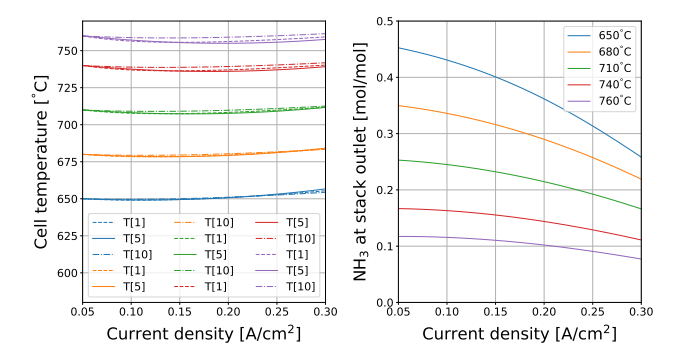


Figure 11. Cell temperature diagram (left) at the first, fifth (which represent the middle section of the cell) and tenth discretisation. Ammonia molar fraction in the anode off gases (right).

the ammonia conversion performance is strongly dependent on temperature; therefore, a higher amount of unconverted ammonia is expected at lower temperatures. This is confirmed by the fact that the experimental polarisation curve at 650°C (Figure 6) shows high concentration losses at high current density due to the low presence of hydrogen and hence lower ammonia conversion efficiency. As the temperature difference between the cells increases due to ammonia decomposition, thermal stress on the cell material is increased, leading to problems in cell operation and reduced lifetime. Installing a mass spectrometer at the end of the stack, makes it possible to quantify the amount of ammonia remaining and thus validate also the conversion performance of the stack. By simulating the operation of the stack for longer periods, the thermal inertia can be assessed, determining the performance at different temperatures, although continuous polarisation and depolarisation tests are not performed due to the need for further details on the test bench.

4 Conclusions and Future Works

The work presented in this paper resulted in the validation of two models built with a lumped pseudo-1D approach: firstly, an ammonia decomposition model built on equations presented and validated in the literature; secondly, a SOFC stack model fed directly with ammonia, built from the structure of a test bench in the laboratory and then validated with the operating parameters used in the laboratory and experimental and polarisation curves. The validated ammonia decomposition reaction model was necessary to implement the ammonia decomposition reaction that occurs within the anode channel of the stack model when it is operated at high temperatures.

The optimal performance of the ammonia decomposition reaction and the ability of the stack model to capture more than 97% of the experimental data, with a maximum relative error of 2.18%, prove the robustness and reliability of the model in investigating the performance of a solid oxide fuel cell stack fed directly with ammonia.

This high accuracy can be further improved by adding some considerations, previously simplified for the purpose of the article, such as recalibrating the ammonia decomposition reaction based on new experimental results or setting up an optimisation problem to obtain optimal values for the area specific resistance ASR_0 and the activation energy E_a ; the same approach could also be used to estimate the best coefficients for the parameters of the activation, ohmic and concentration losses equations neglected in this case study. This would extend the current range of application of the stack. These considerations arise naturally from the fact that the material and geometric structure of the stack are covered by trade secrets. Therefore, this model is intended as a basis for refining the description of the test bench model and enhancing simulation performance.

The model's objective is to obtain a dynamic response from the stack to changes in operating conditions, such as the transition between nominal load and partial load. This enables the prediction of model outputs and the optimisation of stack performance. In addition, this highly accurate model can be used as a basis for scale-up investigations and can be implemented in a Balance of Plant (BoP) model, which represents all components in an industrial plant configuration, including control loops; a highly accurate stack model allows the evaluation of operating parameters to be adopted for optimal plant performance and the optimisation of control strategies in real cases.

Acknowledgements

The project is supported by the Clean Hydrogen Partnership and its members Hydrogen Europe and Hydrogen Europe Research, under Grant Agreement No. 101101521.

References

- Andersson, Daniel et al. (2011). "Dynamic modeling of a solid oxide fuel cell system in Modelica". In: 8th Modelica Conference. DOI: http://dx.doi.org/10.3384/ecp11063593.
- EuropeanCommission (2022). *Green Deal: key to a climate-neutral and sustainable EU*. Tech. rep. International Renewable Energy Agency. URL: https://www.europarl.europa.eu/topics/en/article/20200618STO81513/green-deal-key-to-aclimate-neutral-and-sustainable-eu.
- IEA (2021). Ammonia Technology Roadmap. Tech. rep. International Energy Agency. URL: https://iea.blob.core.windows.net / assets / 6ee41bb9 8e81 4b64 8701 2acc064ff6e4 / AmmoniaTechnologyRoadmap.pdf.
- IRENA (2024). World Energy Transitions Outlook 2024: 1.5°C Pathway. Tech. rep. International Renewable Energy Agency. URL: https://www.irena.org/Publications/2024/Nov/World-Energy-Transitions-Outlook-2024.
- Kishimoto, Masashi et al. (2017-01). "Formulation of ammonia decomposition rate in Ni-YSZ anode of solid oxide fuel cells". In: *International Journal of Hydrogen Energy* 42, pp. 2370–2380. ISSN: 03603199. DOI: 10.1016/j.ijhydene. 2016.11.183.
- Lyu, Zhen-Hua et al. (2023). "Design of ammonia oxidation electrocatalysts for efficient direct ammonia fuel cells". In: *EnergyChem* 5.3, p. 100093. ISSN: 2589-7780. DOI: https://doi.org/10.1016/j.enchem.2022.100093.
- McBride, Bonnie J., Michael J. Zehe, and Sanford Gordon (2002-09). NASA Glenn Coefficients for Calculating Thermodynamic Properties of Individual Species. Tech. rep. NASA. URL: https://ntrs.nasa.gov/citations/20020085330.
- NIST (2023). *NIST Ammonia properties*. Tech. rep. NIST. URL: https://webbook.nist.gov/cgi/cbook.cgi?ID=C7664417.
- Omer, Ahmed et al. (2023-07). "Design and performance optimization of a direct ammonia planar solid oxide fuel cell for high electrical efficiency". In: *Journal of Power Sources* 573, p. 233135. ISSN: 0378-7753. DOI: 10.1016/j.jpowsour.2023. 233135.
- Wan, Zhijian et al. (2021). "Ammonia as an effective hydrogen carrier and a clean fuel for solid oxide fuel cells". In: *Energy Conversion and Management*. ISSN: 0196-8904. DOI: https://doi.org/10.1016/j.enconman.2020.113729.
- Wang, Bin et al. (2022). "Ammonia as a green energy carrier: Electrochemical synthesis and direct ammonia fuel cell a comprehensive review". In: *Fuel Processing Technology* 235, p. 107380. ISSN: 0378-3820. DOI: https://doi.org/10.1016/j.fuproc.2022.107380.
- Zendrini, Michele et al. (2021). "Assessment of ammonia as energy carrier in the use with reversible solid oxide cells". In: *International Journal of Hydrogen Energy*. DOI: https://doi.org/10.1016/j.ijhydene.2021.06.139.
- Zheng, Chunzheng et al. (2023). "Research Status, Optimization Strategies, and Future Prospects of Ammonia Decomposition Catalysts for COx-Free Hydrogen". In: *Industrial & Engineering Chemistry Research*. DOI: https://doi.org/10.1021/acs.iecr.3c01261.